Nuclear Engineering and Technology xxx (xxxx) xxx

Contents lists available at ScienceDirect

Nuclear Engineering and Technology

journal homepage: www.elsevier.com/locate/net

# A study of the $NF_3$ plasma etching reaction with cobalt oxide films grown on an inorganic compounds

Jae-Yong Lee [a, b, *], Kyung-Min Kim [b], Min-Seung Ko [b], Yong-Soo Kim [b]

[a] Korea Radioactive Waste Agency, 19, Chunghyocheon-gil, Gyeongju-si, Gyeongsangbuk-do, South Korea
[b] Department of Nuclear Engineering, Hanyang University, 222, Wangsimni-ro, Seongdong-gu, Seoul, 04763, South Korea

ARTICLE INFO

*Article history:*
Received 14 June 2022
Received in revised form
10 August 2022
Accepted 19 August 2022
Available online xxx

*Keywords:*
Decontamination
Radioactive waste
Cobalt oxide
Plasma etching
Cobalt fluoride

ABSTRACT

In this study, an $NF_3$ plasma etching reaction with a cobalt oxide ($Co_3O_4$) films grown on the surface of inorganic compounds using granite was investigated. Experimental results showed that the etching rate can be up to 1.604 μm/min at 380 °C under 150 W of RF power. EDS and XPS analysis showed that main reaction product is $CoF_2$, which is generated by fluorination in $NF_3$ plasma. The etching rate of cobalt oxide films grown on inorganic compounds in this study was affected by surface roughness and etch selectivity. This study demonstrates that the plasma surface decontamination can effectively and efficiently remove contaminated nuclides such as cobalt attached to aggregate in concrete generated when decommissioning of nuclear power plants.



## 1. Introduction

Although nuclear power is an effective energy source, the permanent shutdown of NPPs (nuclear power plants) has been occurring steadily around the world due to the accident of Fukushima NPPs and the appearance of new renewable energy. Especially, generation of radioactive waste is the most sensitive issue after permanent shutdown of NPPs. Hence, technologies to recycle/reuse of the radioactive waste have been developed and researched, since a large volume of radioactive waste is likely to be generated during decommissioning of NPPs.

It is well known that concrete is basically used a structure in NPPs due to its reasonable cost and neutron shielding. As shown in Table 1, IAEA predicted that a huge amount of radioactive concrete would be generated from decommissioning of nuclear facilities [1]. Specifically, the EC (European Commission) expected that about 500 million tons of concrete waste will be generated in Europe by 2060 due to decommissioning of NPPs [2]. It is known that the radioactive concrete waste consists of surface contaminated concretes and activated concretes. Surface contaminated concretes are generated by imbibition of radioactive liquids from system to concrete, and most activated concretes are produced in biological shields located around the reactor by fast neutrons generated during NPP operation [3]. Therefore, radionuclides are mainly present in cement paste or mortar and are attached to the surface of aggregates in concrete (Fig. 1) [4]. So, if radionuclides from surface of aggregates in concrete can be removed completely using specific techniques, aggregates can be reused or recycled, which can reduce the volume of radioactive concrete.

Decontamination technologies of concrete include chemical methods, thermal methods, and mechanical methods. Chemical methods are wet technologies separating contaminants from concrete using an oxidizing agent/reducing agent, acid/base, gel, and foam [5–22]. In thermal methods, contaminants are removed by explosive fracture in concrete, which is caused by irradiation with high energy using lasers, microwaves, and pulsed power discharge [23–28]. Mechanical methods are most commonly used technologies that physically separate contaminants on the surface of the concrete using milling, scabbling, blasting, vacuum cleaning, and brushing [29–35]. This technology is mainly used in the field, however, caution is needed to prevent workers from inhaling mixture of dusts and radionuclides. Chemical methods and thermal methods still have lack of practical use cases, requiring further research on issue of expensive decontamination costs and generation of secondary waste.

Plasma surface decontamination is an outstanding technology

* Corresponding author. Korea Radioactive Waste Agency, 19, Chunghyocheon-gil, Gyeongju-si, Gyeongsangbuk-do, South Korea.
*E-mail address:* chungooc@korad.or.kr (J.-Y. Lee).

https://doi.org/10.1016/j.net.2022.08.020

**Table 1**
Typical radioactive waste generated from decommissioned nuclear power plants [1].

| Radioactive waste generation | 250 MW(e) GCR (t) | 900–1300 MW(e) PWR (t) | Reprocessing plant 5 t/d throughput (t) |
|---|---|---|---|
| Irradiated carbon steel | 3000 | – | – |
| Activated steel | – | 650 | – |
| Graphite | 2500 | – | – |
| Activated concrete | 600 | 300 | – |
| Contaminated ferrite steel | 6000 | 2400 | – |
| Steel likely to be contaminated | – | 1100 | 3400 |
| Contaminated concrete | 150 | 600 | 1850 |
| Contaminated lagging | 150 | 150 | 400 |
| Contaminated technological wastes | – | 1000 | 300 |

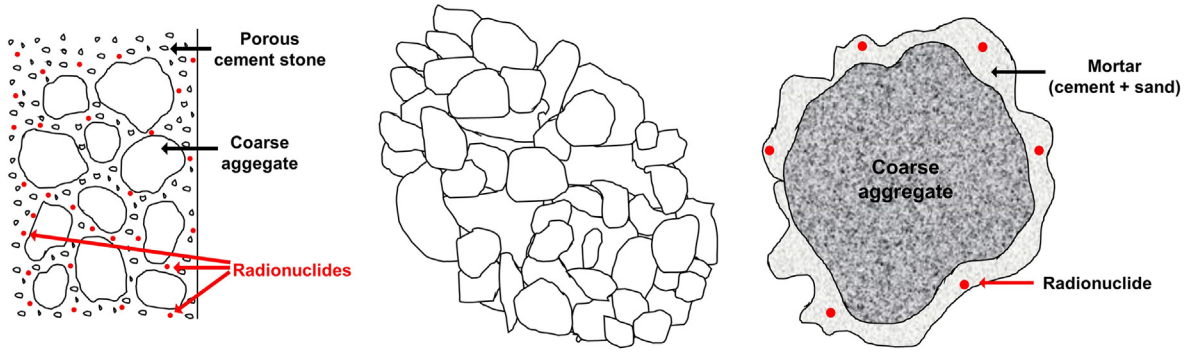


**Fig. 1.** Schematics of contaminated concrete, aggregate after recycling process of concrete and cross section of aggregate after recycling process of concrete.

using plasma etching that effectively removes surface contaminants and produces less secondary waste than other chemical methods. Many researchers have demonstrated the removal of contaminants from the metal surface, and it is a critical technology for reducing volume of radioactive waste generated when decommissioning of NPPs [36–48]. However, studies on plasma surface decontamination of concrete, which occupy the largest amount of radioactive waste generated when decommissioning of NPPs, have not been sufficient.

In fact, cobalt is the most common contaminated nuclides in radioactive concrete generated when decommissioning of NPPs [3]. Cobalt exists in various chemical forms ($Co^{2+}$, $Co^{3+}$, $CoCO_3$, $Co(OH)_3$, $Co_3O_4$), which is attached to the surface of aggregates in concrete [49], however, it is predicted to be converted into cobalt oxide ($Co_3O_4$) through mixed technologies using heating and milling, which is a conventional recycling process of separating mortar and aggregate in concrete [50,51]. However, it is necessary to remove specific contaminants on the aggregate through plasma surface decontamination since this technology increases the amount of secondary waste by polishing the aggregate.

To demonstrate a high etching rate for radioactive cobalt isotopes on the surface of aggregates after conventional recycling processes, the etching reaction of cobalt oxide films grown on inorganic compound was investigated in this study using $NF_3$ plasma. In parallel, surface analysis was performed to understand mechanism between cobalt oxide and $NF_3$ plasma with two experimental parameters: temperature, and power.

## 2. Experimental

### 2.1. Growth of cobalt oxide films on inorganic compounds

The actual specimen is presumed to have a nuclide attached to the surface of the aggregate to which the mortar is bound. However, in this experiment, assuming that the mortar was almost removed after the concrete decontamination including milling and heating, a specimen with a nuclide attached to the surface of the aggregate was manufactured.

It is well known that aggregate is composed of inorganic compounds. First, the cobalt oxide films were prepared on inorganic compounds using granite (31 mm in length, 31 mm in width, and 5 mm in thickness). Specimens were polished with sandpaper with 320, 600, and 1200 grit and then were cleaned using distilled water in an ultrasonic cleaner. Samples were dried using an air gun after polishing, and then a cobalt nitrate (II) hexahydrate ($Co(NO_3)_2 \cdot 6H_2O$) solution with concentration of 300 mg/mL was applied on their surfaces. Next, these samples were baked in an electrical furnace at 500 °C for 3 h to grow cobalt oxide films on the surface of the inorganic compounds using granite.

### 2.2. Design of plasma etching equipment

A diagram of the plasma etching equipment used in this experiment is shown in Fig. 2. The vacuum chamber with a volume of 8 L was made of stainless steel, and the inner surface was electropolished to prevent corrosion. Etching gas was continuously and accurately supplied to the showerhead in the vacuum chamber through a MFC (mass flow controller). The sample on the cover was heated using a heater that can go up to 1000 °C, and a thermocouple was placed on the surface of the sample to measure the surface temperature in the vacuum chamber. To prevent corrosion of the vacuum chamber at high temperature, a cooling water was continuously circulated in the upper part and lower part of the vacuum chamber. To generate plasma, the plasma source used RF (radio frequency) power up to 600 W at 13.56 MHz. The distance between the showerhead attached to the top of the chamber and the sample on the cover can be adjusted up to 150 mm. The plasma state was visually observed during the experiment through a

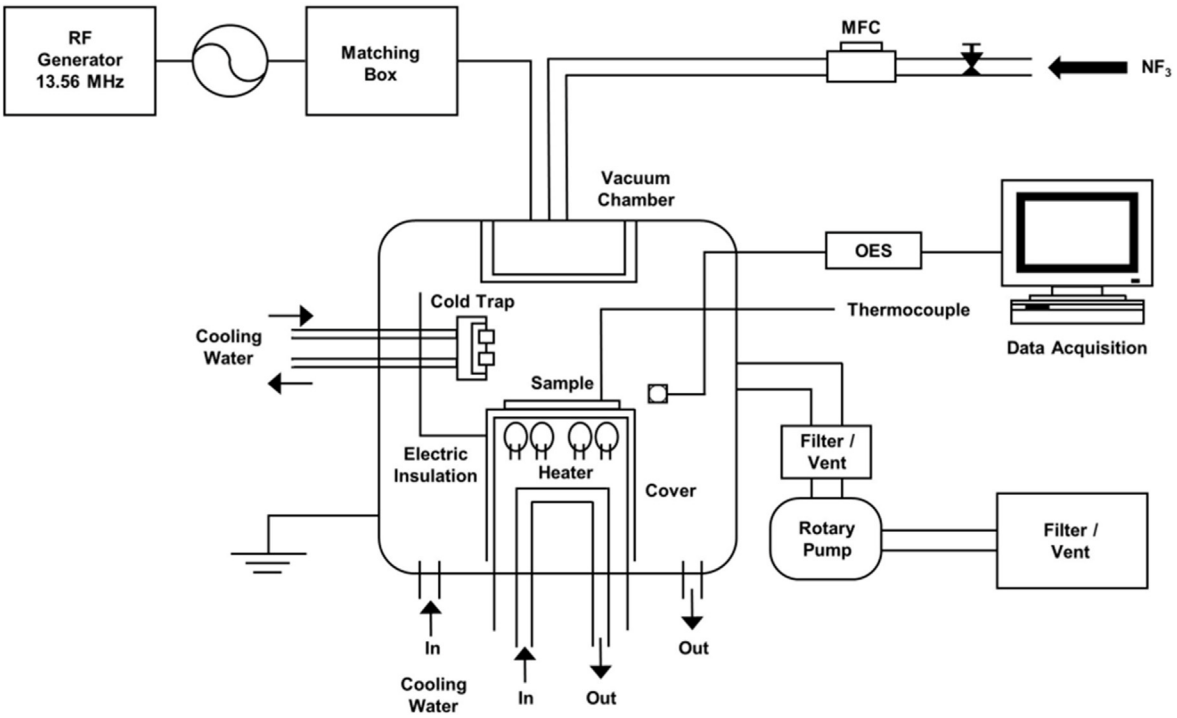


**Fig. 2.** Schematics of plasma etching machine.

viewpoint in the vacuum chamber, and the plasma environment was analyzed using OES (optical emission spectroscopy). A cold trap was installed in the vacuum chamber to collect and identify the reaction product. To minimize the exposure to the external environment, the cold trap was transferred for XPS analysis using a desiccator and a VTM (vacuum transfer module) (Fig. 3).

### 2.3. Plasma etching experiments

To remove impurities and moisture residue on the wall of the vacuum chamber, the vacuum chamber was baked prior to the plasma etching experiment. Total pressure in the vacuum chamber was maintained at 0.3 Torr, and the flow rate of $NF_3$ gas was fixed at 15 sccm (standard cubic centimeters per minute) using MFC. The distance between the showerhead and cover was fixed at 40 mm. The total reaction time was 3 min, and specimen weights were measured every 0.5 min.

Plasma etching experiments were conducted at two RF powers (150 W and 220 W) at various temperature (300 °C, 330 °C, 350 °C, and 380 °C). Etching rate was determined using the weight loss of the specimen during the plasma reaction to evaluate of thickness change on the surface of the specimen. The weight change of the specimen was measured using an electronic micro balance (model BP210D, Sartorius) with readability of $10^{-5}$ g.

Surface analysis of specimens was carried out using OM (optical microscopy), SEM (scanning electron microscopy), EDS (energy dispersive x-ray spectroscopy), XRD (x-ray diffraction), and XPS (x-ray photoelectron spectroscopy).

## 3. Results and discussion

### 3.1. Analysis of optical plasma diagnostics

Vacuum baking was conducted prior to the experiment at temperature of 300 °C to remove moisture and particles inside the vacuum chamber. The diagnostic using OES showed F peaks (685, 703 nm) [45] and $N_2$ peaks (337, 357, 400 nm) [52] without the presence of $OH^-$ peak (309 nm) [53–55] which are generated due

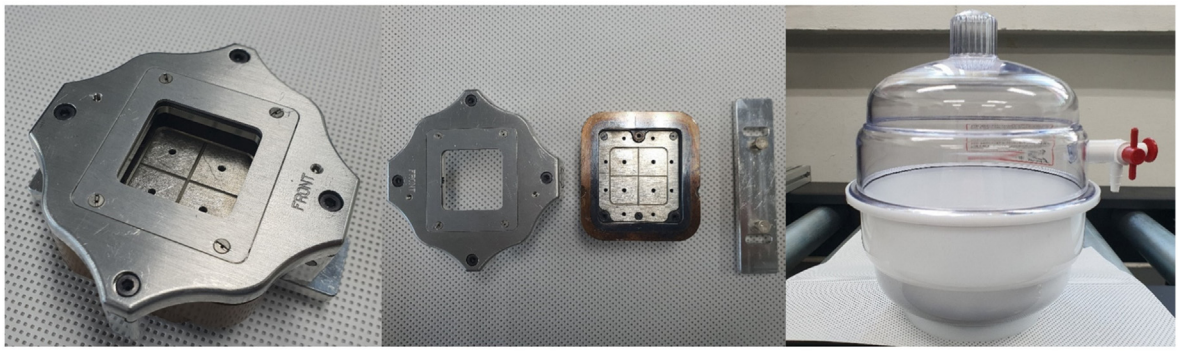


**Fig. 3.** Images of VTM (vacuum transfer module), parts of VTM, and desiccator.

to dissociation of moisture during the plasma reaction (Fig. 4). Therefore, the results confirmed that F radicals were sufficiently produced due to effective dissociation of $NF_3$ in the plasma.

### 3.2. Surface analysis before and after plasma reaction

XRD analysis showed that the peaks of cobalt oxide films on the surface of the inorganic compounds were in the same position as the peaks of $Co_3O_4$ manufactured by Aldrich (Fig. 5). This results confirm that $Co_3O_4$ films were grown on the inorganic compounds. Also, as shown in Fig. 6, the $Co_{2p}$ binding energy peak at 780.1 eV was clearly observed in the XPS analysis, demonstrating $Co_3O_4$ films formed on the surface of the inorganic compounds. This result is consistent with thermodynamic predictions that the formation of $Co_3O_4$, which has the properties listed in Table 2, is advantageous at temperatures below 900 °C [50,56].

OM and SEM were conducted to observe the change in the surface of $Co_3O_4$ films grown on the inorganic compounds before and after the reaction. As shown in Fig. 7, micrograph shows that $Co_3O_4$ films were removed from the surface, resulting in a change in the surface of inorganic compounds. Also, SEM results demonstrated that $Co_3O_4$ films were removed because the surface of inorganic compounds was only observed when the plasma reaction was completed (Fig. 8).

### 3.3. Analysis of reaction product

According to studies on reaction between cobalt and plasma using $CF_4$–$O_2$ and $SF_6$–$O_2$, it is expected that the overall etching reaction involved that carbonylation and fluoro-carbonylation [41,44,45] would occur due to the low melting point of cobalt carbonyl and the high melting point of cobalt fluoride. However, recent findings showed that the fluorination is the principal reaction between cobalt and plasma using $CF_4$–$O_2$, $SF_6$–$O_2$, and $NF_3$ [46–48].

As shown in Fig. 9, EDS results for the specimen mean that the surface of base material is revealed after plasma reaction. The result shows that $Co_3O_4$ films were completely removed after the plasma reaction, and a small amount of cobalt fluoride remained on the surface of inorganic compounds.

XPS analysis was conducted to identify reaction products generated by reacting with $NF_3$ plasma and $Co_3O_4$ films on the inorganic compounds. To confirm the chemical form of the reaction product, condensed reaction products were collected using the cold trap made of copper.

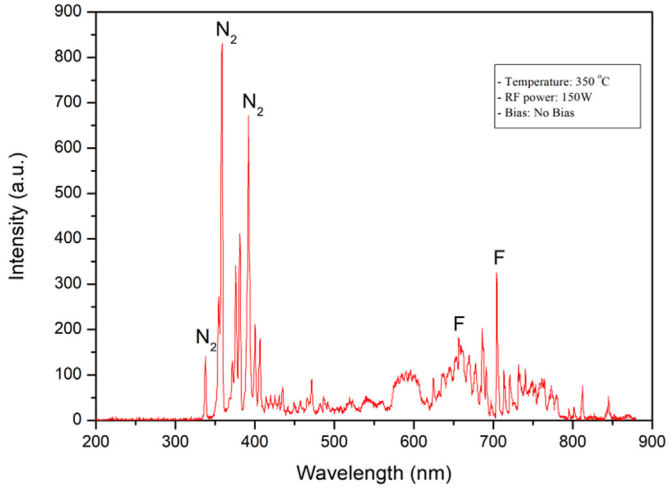


**Fig. 4.** OES peak during $NF_3$ plasma reaction.

Cobalt fluoride can exist in two forms, $CoF_2$, $CoF_3$ [45,57,58], which easily bond to water in normal environments. Therefore, since the polarity of cobalt fluoride and water was similar, it was confirmed that the specimen and moisture were easily combined, and then the peak was moved in the XPS analysis. It was difficult to confirm the reaction product in previous studies because cobalt fluoride showed a chemical form of $CoF_2 \cdot nH_2O$ with a $Co_{2p}$ binding energy at 782.6 eV [48]. Therefore, to minimize moisture adsorption of the specimen, the specimen was transported to the XPS analysis laboratory in various ways. The cold trap was transferred using a petri plate, a vial with silica gel, a vial with argon gas (Fig. 10), and a VTM in the desiccator (Fig. 3).

As shown in Fig. 11, the XPS results confirmed that the $Co_{2p}$ binding energy of $CoF_2 \cdot nH_2O$ at 782.6 eV when a specimen was transported using a petri plate, a vial with silica gel, and a vial with argon gas. This result means that the specimen was exposed to air during transportation after plasma reaction.

However, the $Co_{2p}$ binding energy was 782.9 eV (Fig. 12) when the specimen was moved using VTM. Since the binding energies of $CoF_2$ and $CoF_3$ are known at 783.0 eV and 782.4 eV, respectively, it is estimated to be $CoF_2$ because it is a difference in energy of the tolerance of $Co_{2p}$ binding energy in this XPS analysis [59,60]. Even if $CoF_3$ formed, the reactivity is high enough to be decomposed immediately after exposure to moisture, and pure $CoF_3$ is not significantly produced in the fluorination reaction [61]. Therefore, the principal reaction product of $Co_3O_4$ films on inorganic compounds using $NF_3$ plasma is likely $CoF_2$.

### 3.4. Plasma etching rate of cobalt oxide

#### 3.4.1. Effect of temperature

In our experiment on cobalt oxide films on inorganic compounds exposed to plasma etching, the weight of the specimen decreased in proportion to etching time. Unlike previous studies [38,40,48], it seems that continued removal of cobalt-fluorine intermediates was affected by the limited amount of cobalt atoms in thin films and the characteristics of the base material.

Removal of the adsorbed cobalt-fluorine intermediates in the plasma etching reaction between cobalt atom and $NF_3$ plasma may be expressed by an exponential function as in previous studies [48]. Since it follows a linear kinetics law, the etching rate of cobalt oxide, $R(t)$, can be expressed:

$$R(t) = k_d[A^*] = k_d[A^*]_0 e^{-\lambda t} - B$$

Here, $k_d$ is the desorption reaction rate constant, $[A^*]$ is the concentration of adsorbed intermediate species on surface of materials, $[A^*]_0$ is the initial concentration of $[A^*]$, $t$ is reaction time in plasma, and $\lambda$ is the reciprocal of characteristic time. Therefore, the initial etching rate, $R = k_d[A^*]_0$ is constant, and can be calculated using the linear slope (characteristic time) from an exponential graph. It is reasonable that same initial etching rates were observed for cobalt oxide films on inorganic compounds and cobalt oxide films on Inconel (Table 3) [48] because the same reaction product ($CoF_2$) is generated for reactions between cobalt oxide and $NF_3$ plasma. Therefore, it is estimated that the etching rate of cobalt oxide films on inorganic compounds is decreased by external effect factor $B$, which is the factor related to the base material, and is described in Sections 3.3.3 and 3.3.4.

To investigate the effect of temperature on the etching rate of cobalt oxide on inorganic compounds, plasma etching experiments were conducted at 300 °C, 330 °C, 350 °C, and 380 °C with the RF power fixed to 150 W. The etching rates were 0.734 μm/min,

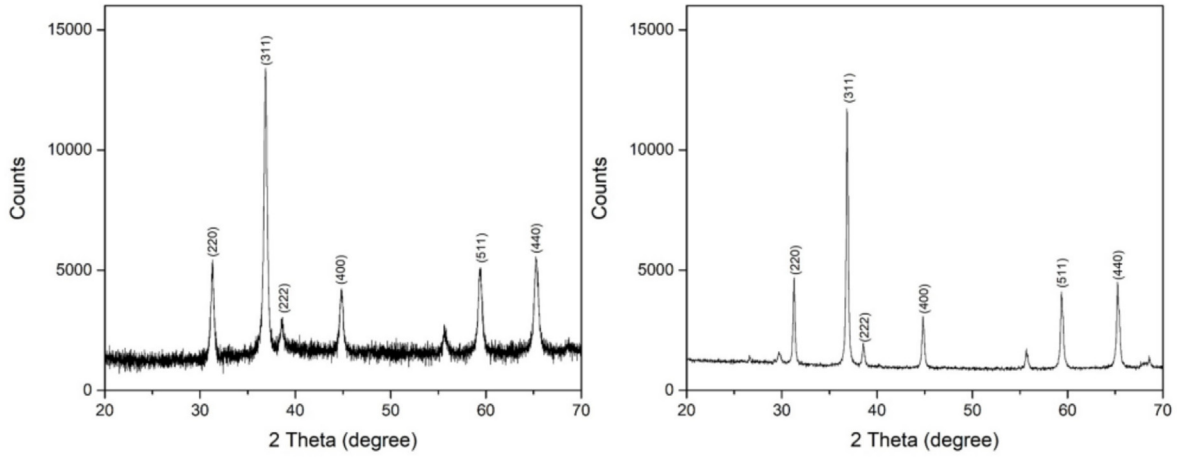


**Fig. 5.** Comparison of XRD peaks between cobalt oxide (sigma aldrich) and cobalt oxide films on inorganic compounds.

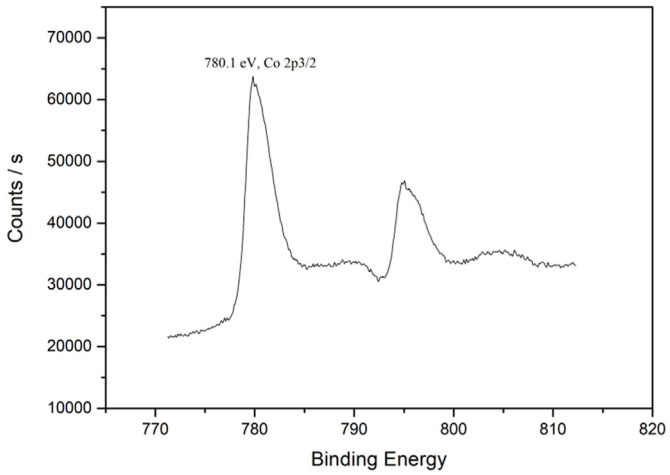


**Fig. 6.** $Co_2p$ binding energy of cobalt oxide films on inorganic compounds using XPS.

**Table 2**
Properties of cobalt (II, III) oxides.

| Properties | |
|---|---|
| Chemical formula | $Co_3O_4$<br>$CoO \cdot Co_2O_3$ |
| Molar mass | 240.80 g/mol |
| Appearance | black solid |
| Density | 6.11 g/cm$^3$ |
| Melting point | 895 °C |
| Boiling point | 900 °C (decomposes) |
| Solubility in water | insoluble |

1.129 μm/min, 1.202 μm/min, and 1.604 μm/min for temperature of 300 °C, 330 °C, 350 °C, and 380 °C (Fig. 13). The results differed from plasma etching rate of the metallic cobalt and cobalt oxide films on Inconel based metal.

### 3.4.2. Effect of RF power

When RF power increased from 150 W to 220 W at a temperature of 350 °C, the etching rate changed from 1.202 μm/min to 1.570 μm/min, and increased by approximately 76% (Fig. 14). In the analysis using OES (Fig. 15), the etching rate is expected to increase because the density of fluorine radical increases with increasing RF power [62,63]. Since the electron density and average electron energy associated with the density of fluorine radicals depends on RF power as the source of plasma generation, fluorine radicals were significantly increased by ionization, excitation, and dissociation of gas molecules. In addition, the etching rate can be further improved if the kinetic energy of reactive ions is increased.

### 3.4.3. Effect on surface roughness of base material

The difference in etching rate of cobalt oxide between the Inconel [48] and inorganic compounds is likely due to the difference in the surface shape of the base material. Because in XPS analysis after each plasma reaction, the reaction products were confirmed in the same chemical form. Unlike the surface of Inconel, thickness of cobalt oxide films is not uniform since the surface of the inorganic compounds is mostly composed of trenches or valleys (Fig. 16). As shown in the SEM image (Fig. 17), by-products are re-deposited in trenches or valleys of inorganic compounds after the plasma reaction in this experiment. The re-deposition of by-products increased in trenches or valleys during the plasma reaction [64,65], which affects the etching rate of the cobalt oxide films as shown in Fig. 18.

### 3.4.4. Effect on etch selectivity of base material

Since inorganic compounds are granite mostly composed of $SiO_2$ and $Al_2O_3$, the difference in etching rates is likely because the etch selectivity of the Inconel and the inorganic compounds was different [66].

$$\text{Etch selectivity} = \text{Etching rate of the etch target}/\text{Etching rate of the base material}$$

Since etch selectivity implies a non-selective etching phenomenon, there were the differences in the etching rate of $Co_3O_4$ films

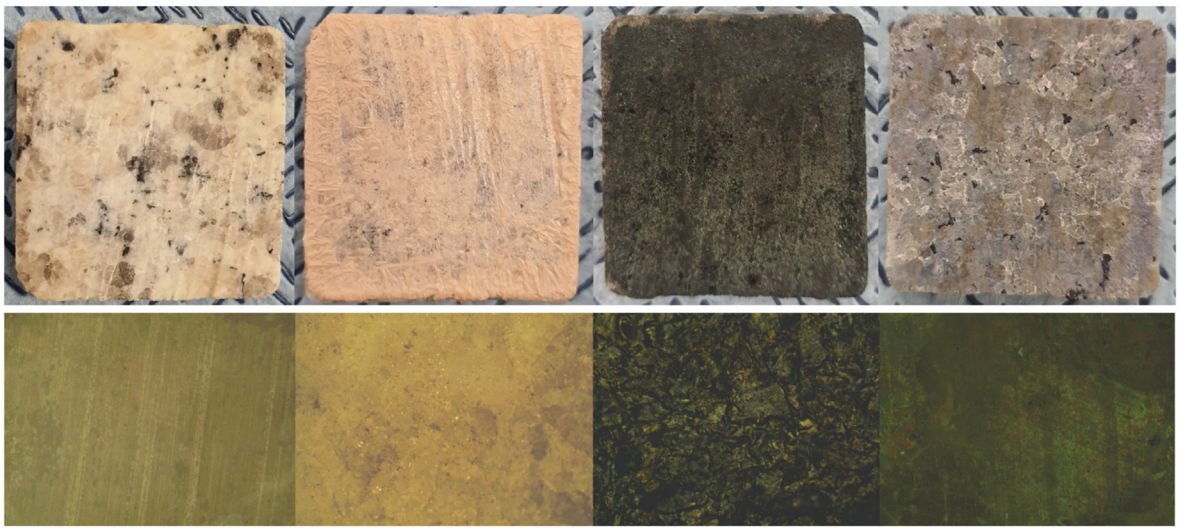

**Fig. 7.** OM images of inorganic compounds, cobalt nitrate on inorganic compounds, and cobalt oxide films on inorganic compounds before and after reaction.

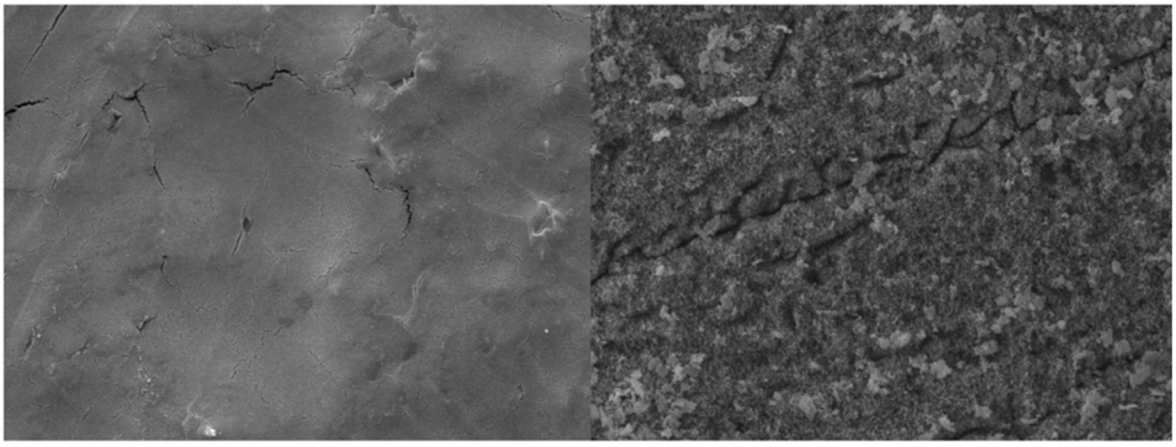

**Fig. 8.** SEM images of cobalt oxide films on inorganic compounds before and after reaction.

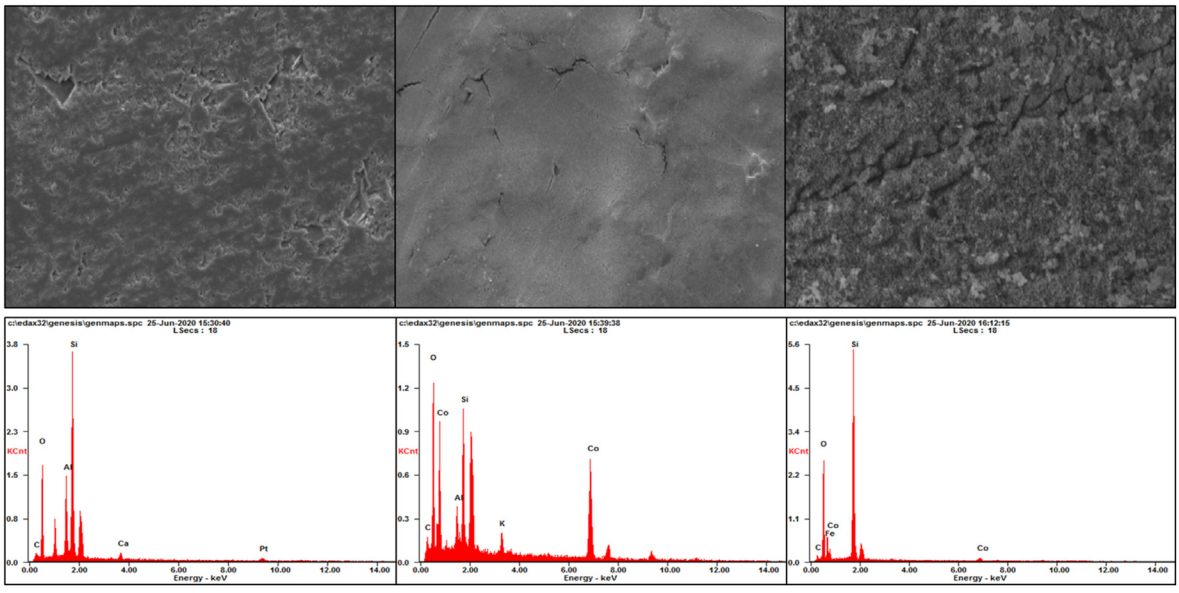


**Fig. 9.** EDS of inorganic compounds, cobalt oxide films on inorganic compounds before and after reaction.

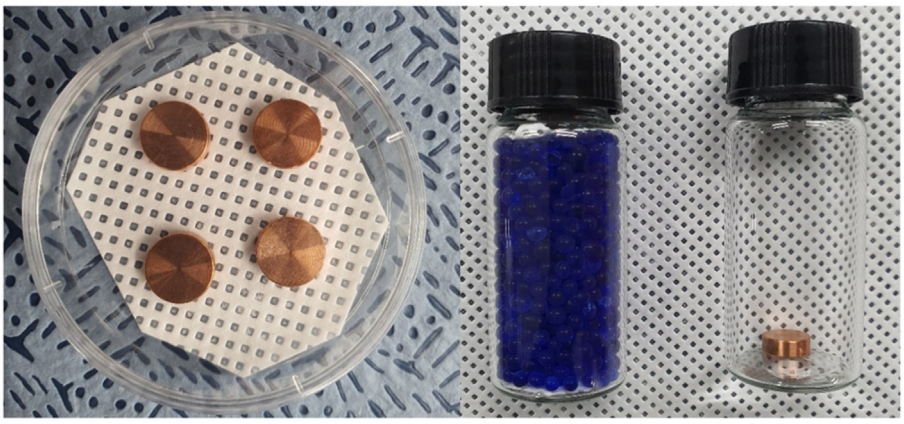

**Fig. 10.** The images of a petri plate, a vial with silica gel, and a vial with argon gas.

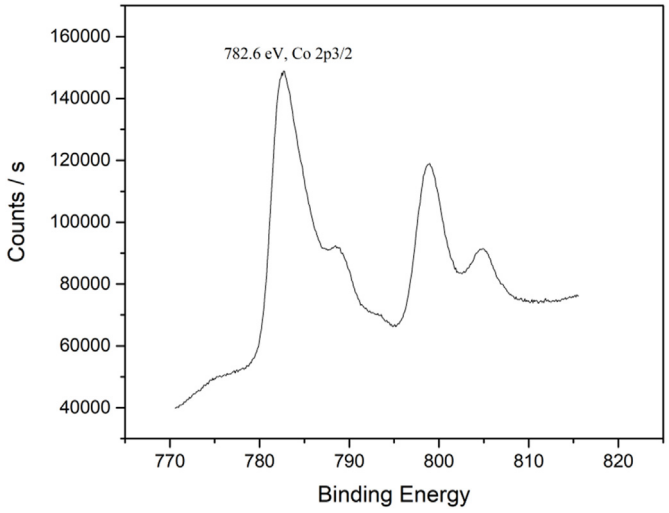


**Fig. 11.** The $Co_2p$ binding energy of cold trap after plasma reaction using petri plate, vial with silica gel, and vial with argon gas.

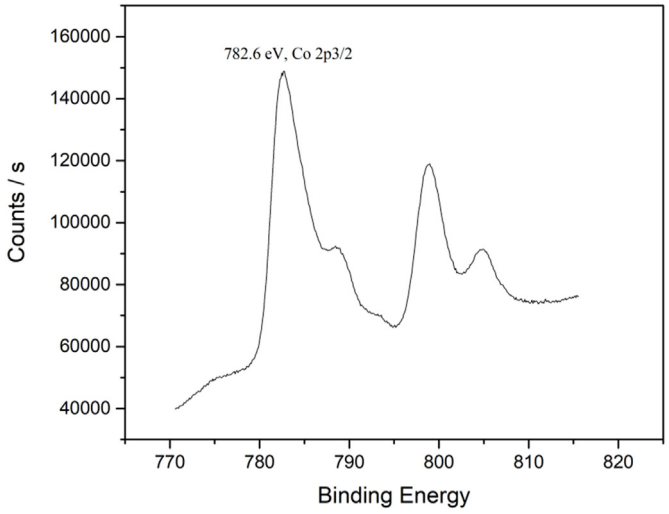


**Fig. 12.** The $Co_2p$ binding energy of cold trap after plasma reaction using VTM and desiccator.

**Table 3**
Initial plasma etching rates of cobalt oxide on Inconel [48].

| Temperature (°C) | RF power (W) | DC Bias (V) | Initial etching rate (μm/min) |
|---|---|---|---|
| 300 | 150 | No | 0.9171 |
| 330 | 150 | No | 1.0622 |
| 350 | 150 | No | 1.3977 |
| 350 | 220 | No | 2.6340 |
| 350 | 220 | −300 | 3.3620 |
| 380 | 150 | No | 5.0967 |
| 410 | 150 | No | 6.8444 |

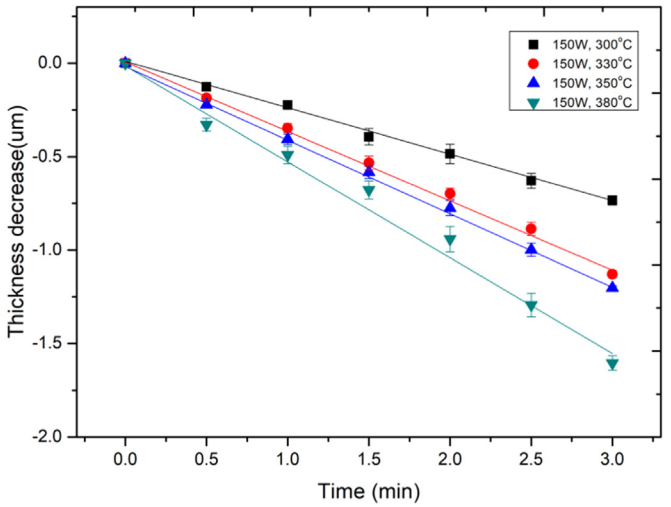


**Fig. 13.** Thickness decrease of cobalt oxide on inorganic compounds at various temperature with an RF power of 150 W.

based on the difference in the base material. The reaction product was generated in some components of the inorganic compounds by the expected fluorination reaction as follows:

$$SiO_{2(s)} + F_{(g)} \rightarrow SiF_{4(g)}$$

$$Al_2O_{3(s)} + F_{(g)} \rightarrow AlF_{3(s)}$$

Very little spontaneous reaction between $SiO_2$ and fluorine occurs without ion bombardment at room temperature [67].

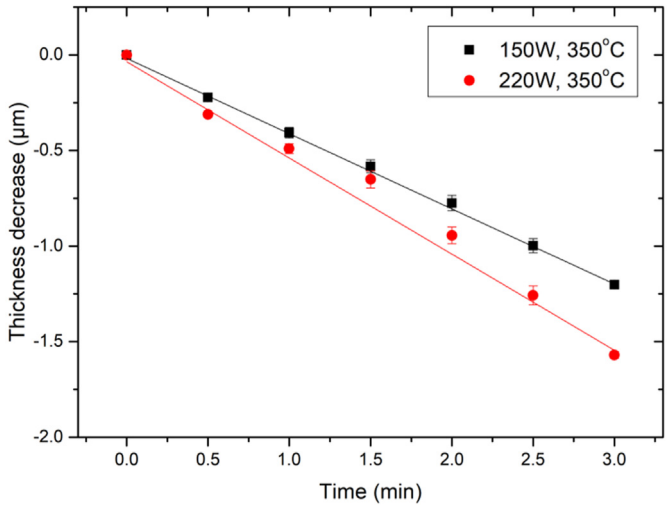


**Fig. 14.** Thickness decrease of cobalt oxide on inorganic compounds at RF power of 150 W and 220 W.

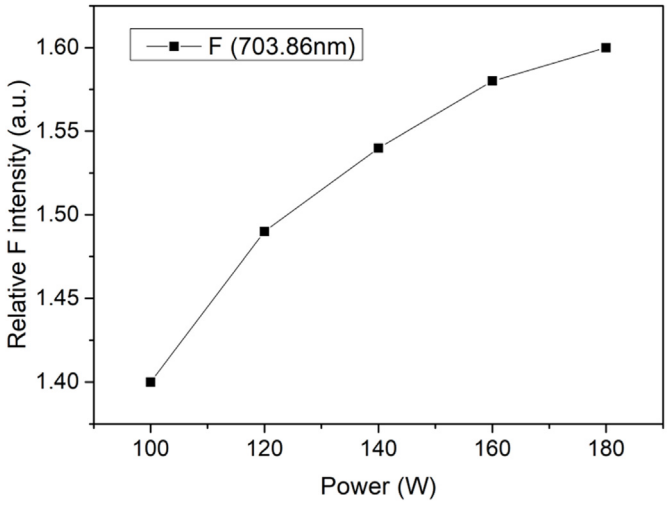


**Fig. 15.** F intensity in plasma reaction at various power using OES.

Furthermore, etching of $Al_2O_3$ is difficult due to the production of $AlF_3$, which remains on the surface as a non-volatile material [68]. XPS results of the cold trap after the plasma reaction showed that the cobalt and fluorine were mostly involve in the fluorination reaction (Fig. 19).

As shown in Fig. 20, it was confirmed that Al did not become a volatile product through a difference between the Si peak (104.1 eV, $SiO_2$) of cold trap after the experiment and the Si peak (102.6 eV, $SiO_2$&$Al_2O_3$) of the surface of the inorganic compound before the experiment. It is estimated that the Si peak of cold trap is generated by decomposition of $SiF_4$. The $SiF_4$ has high reactivity that it decomposed as soon as it bonded to water [59,60]. It is estimated that $SiO_2$, the main component of the inorganic compounds, was partially etched through a spontaneous reaction. However, the etching of the inorganic compounds was disturbed by the generation of non-volatile product such as $AlF_3$. Therefore, the main reaction in this experiment was cobalt-fluorination.

### 3.5. Proposed plasma-surface interaction of the cobalt oxide films

In this study, the $Co_3O_4$ films on the inorganic compounds were removed by forming $CoF_2$, which is a volatile product generated by plasma-surface interactions. The OES peak shows that only fluorine radicals are generated as reactive radicals in the $NF_3$ plasma. Therefore, the etching of $Co_3O_4$ films using $NF_3$ plasma is proposed as a fluorination reaction having the following overall reaction:

$$Co_3O_{4(s)} + 6F_{(g)} \rightarrow 3CoF_{2(g)} + 4O_{(g)}$$

Previous studies on the fluorination mechanism using $NF_3$ plasma have demonstrated that $[CoF\bullet nO_{(ad)}]^*$ is formed on the surface and is in balance with the surface atoms. When the fluorine radical in $NF_3$ plasma successfully interacted with the intermediate species (e.g., cobalt-fluorine-oxygen compounds), the reaction products (e.g., $CoF_2$) formed and desorbed from the surface. Therefore, the kinetic scheme of the plasma reaction can be expressed as follows:

$$[Co_3O_4] \underset{k_a}{\overset{k_d}{\rightleftarrows}} [CoF_{(ad)} \cdot nO]^* \xrightarrow{k^*} CoF_{2(g)}$$

When $k^* > k_a$, the desorption rate becomes constant, and then $R_d = k_d[CoF_{(ad)}.nO]^*$ is explained. Therefore, this overall reaction can be described by the following basic reactions:

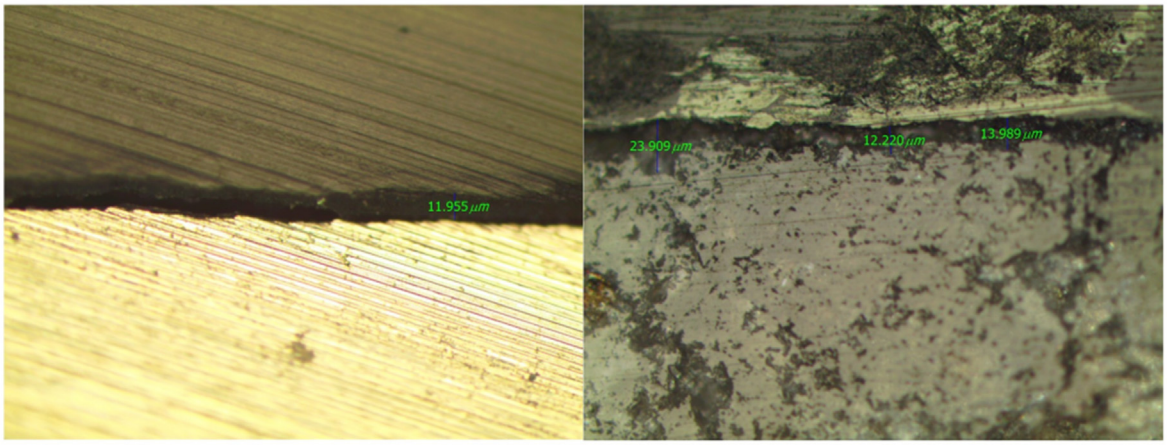


**Fig. 16.** Comparison of cross section between cobalt oxide films on Inconel and cobalt oxide films on inorganic compounds.

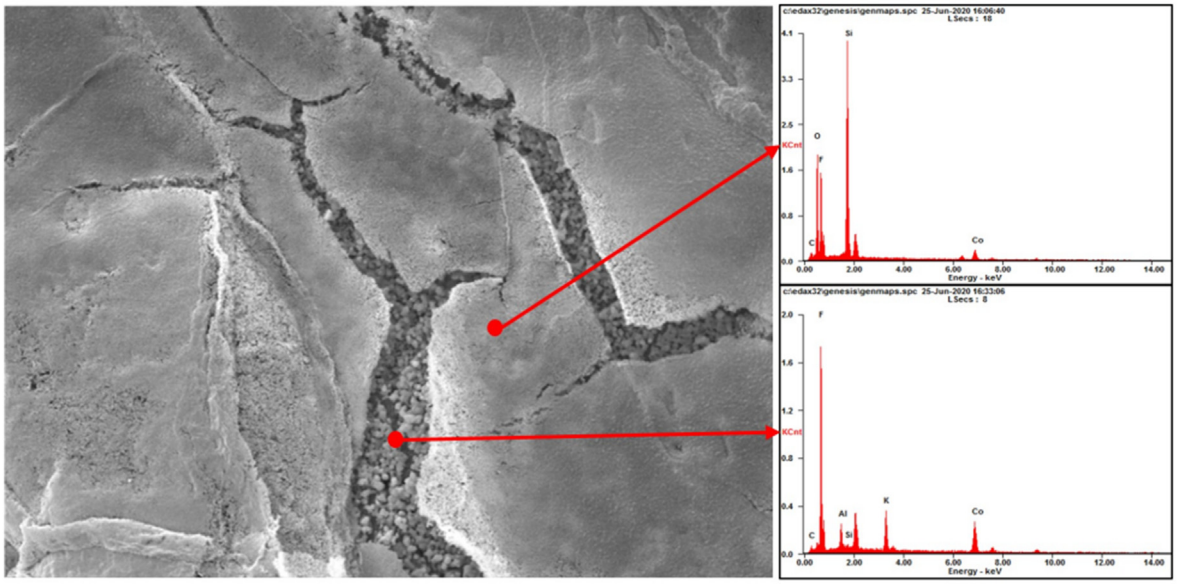


**Fig. 17.** SEM images of valley or trench in cobalt oxide films on inorganic compounds after reaction.

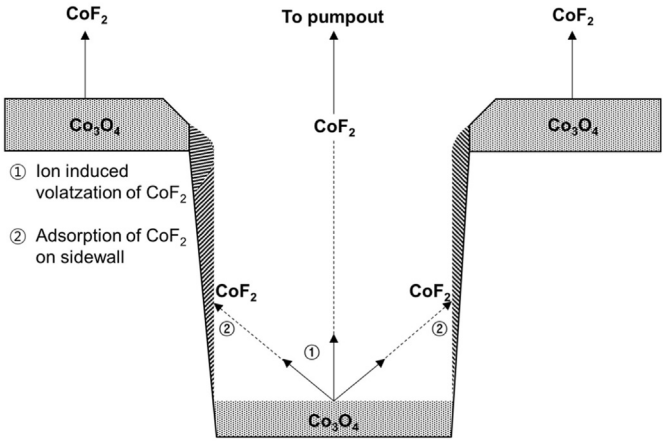


**Fig. 18.** Roughness effect of cobalt oxide films on inorganic compounds.

$$Co_3O_{4(s)} + F_{(g)} \rightarrow CoF_{(ad)} \cdot nO^*$$

$$CoF_{(ad)} \cdot nO^* + F_{(g)} \rightarrow CoF_{2(g)} + nO$$

## 4. Conclusions

According to the predicted volume of IAEA, 900 tons of radioactive concrete wastes will be generated during the decommissioning of PWR (pressurized water reactor) with 900–1300 MWe. Radioactive concretes largely consist of surface-contaminated concretes generated by imbibition of radioactive liquids in the system and activated concretes generated by fast neutrons in the biological shields surrounding the reactor. In fact, most contaminated isotopes are present in cement paste or mortar

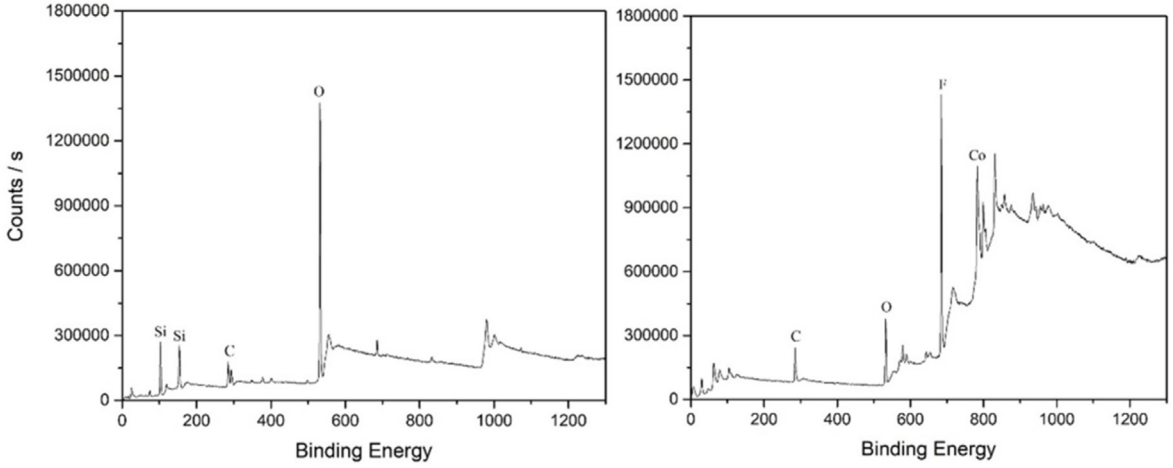


**Fig. 19.** Total peak of inorganic compounds and cold trap after reaction using XPS.

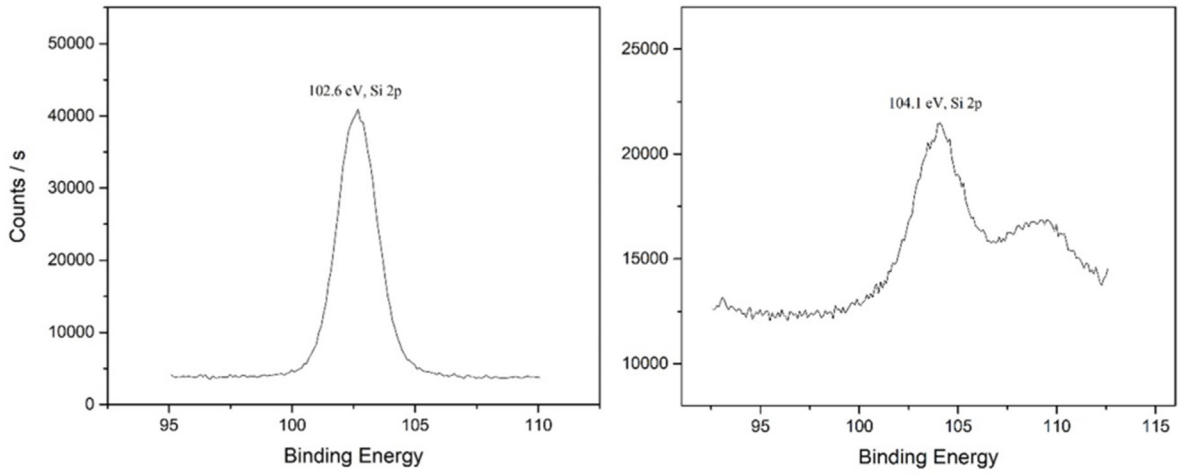


**Fig. 20.** Si2p binding energy of inorganic compounds and cold trap after reaction using XPS.

in concrete. Especially, $^{58}Co$ and $^{60}Co$ are representative radionuclides that attach to the surfaces of aggregate in the concrete. Therefore, it is necessary to develop effective surface decontamination technologies to remove surface-contaminated nuclides and to generate less secondary waste.

Plasma surface decontamination is a removal technology that uses plasma etching to remove effectively surface contaminants, generating less secondary waste than other chemical methods. In this study, the $NF_3$ plasma etching reaction with cobalt oxide ($Co_3O_4$) films grown on the inorganic compounds was investigated to demonstrate the etching of cobalt attached on aggregate in concrete for practical application.

This experiments demonstrated that etching rate can be up to 1.604 μm/min at 380 °C under 150 W of RF power. Therefore, if power and temperature in the vacuum chamber are sufficient increased, the practical available etching rates may reach 3.0 μm/min. Also, the result of cobalt oxide films on inorganic compounds confirmed that the etching rate of cobalt oxide is affected by surface roughness and etch selectivity of the base material.

Although the etching rate of cobalt oxide was influenced by the base material, XPS analysis demonstrated that the main reaction product is $CoF_2$ through the fluorination reaction. Therefore, the surface etching reaction of $Co_3O_4$ using $NF_3$ plasma is proposed as a fluorination reaction having the following overall reaction:

$$Co_3O_{4(s)}+6F_{(g)} \rightarrow 3CoF_{2(g)}+4O_{(g)}$$

Desorption of cobalt-fluorine-oxygen compounds such as intermediate species occurs when interacting with fluorine radicals produced in $NF_3$ plasma. Therefore, the desorption rate becomes constant, and $R_d = k_d[CoF_{(ad)}.nO]^*$, following the linear kinetic law. Also, the surface coverage of intermediate species can be limited by the continuous reaction of thin cobalt oxide films. Therefore, despite the desorption of cobalt fluorides follows a linear kinetic law, the weight of the specimen should decrease without being proportional to the reaction time. However, the weight of specimen decreased according to the reaction time due to the influence of the base material in this experiment.

In conclusion, the result of this study demonstrated that plasma surface decontamination effectively and efficiently removes contaminated nuclides such as cobalt attached to aggregate existing in radioactive concrete generated when decommissioning of NPPs.

## Declaration of competing interest

The authors declare the following financial interests/personal relationships which may be considered as potential competing interests:

Yong-Soo Kim reports financial support was provided Korea Institute of Energy Technology Evaluation and Planning(KETEP). Kyung-Min Kim reports financial support was provided by Korea Institute of Energy Technology Evaluation and Planning(KETEP). Jae-Yong Lee reports financial support was provided by Korea Institute of Energy Technology Evaluation and Planning(KETEP).

## Acknowledgements

This work was supported by a Korea Institute of Energy Technology Evaluation and Planning(KETEP) and the Ministry of Trade, Industry & Energy(MOTIE) of the Republic of Korea (No. 20191510301300) and by the Human Resources Program in Energy Technology of the Korea Institute of Energy Technology Evaluation and Planning (KETEP), granted financial resources from the Ministry of Trade, Industry, & Energy, Republic of Korea (No. 20184030201970).

## References

[1] IAEA, Managing low radioactivity material from the decommissioning of nuclear facilities, in: TECHNICAL REPORTS, IAEA, VIENNA, 2008, p. 201.
[2] U.S. Chung, et al., Current Status of Decommissioning Projects and Their Strategies in Advanced Countries, Korea, Republic of, 2007, p. 236.
[3] M. Snyder, Characterization and Remediation of Contaminated Concrete, Electric Power Research Institute, 2015, p. 158.
[4] Y. Min Byung, et al., Separation of radionuclide from dismantled concrete waste, J. Korean Radioact. Waste Soc. 7 (2) (2009) 79–86.
[5] R. Castellani, et al., Efficiency enhancement of decontamination gels by a superabsorbent polymer, Colloids Surf. A Physicochem. Eng. Asp. 454 (2014) 89–95.
[6] W.S. Kim, et al., Effect of particle-size distribution on chemical washing experiment of uranium contaminated concrete, in: Proceedings of the KNS Autumn Meeting, KNS, Korea, Republic of, 2011.
[7] A. Jestin, et al., A concrete bio-decontamination process in nuclear substructures: effects of organic acids, in: EUROCORR 2004: Long Term Prediction and Modeling of Corrosion, France, 2004.
[8] D. Gurau, R. Deju, The use of chemical gel for decontamination during decommissioning of nuclear facilities, Radiat. Phys. Chem. 106 (2015) 371–375.
[9] M.D. Kaminski, M.R. Finck, C.J. Mertz, Composition Suitable for Decontaminating a Porous Surface Contaminated with Cesium, Google Patents, 2010.
[10] M. Koh, et al., Surface decontamination of radioactive metal wastes using acid-in-supercritical CO2 emulsions, Ind. Eng. Chem. Res. 47 (2) (2008) 278–283.

[11] M.T. Harris, D.W. DePaoli, M. Ally, Modeling the electrokinetic transport of strontium and cesium through a concrete disk, Separ. Purif. Technol. 11 (3) (1997) 173–184.
[12] M.T. Harris, D.W. DePaoli, M.R. Ally, Modeling the electrokinetic decontamination of concrete, Separ. Sci. Technol. 32 (1–4) (1997) 827–848.
[13] J. Tripp, et al., Cleaning and decontamination using strippable and protective coatings at the Idaho national engineering and environmental laboratory, in: Conference: Waste Management '99, US, Tucson, AZ, 02/28/1999–03/04/1999, p. 8. Other Information: PBD: 1 Mar 1999. 1999: United States. p. Medium: P; Size.
[14] W.D. Bostick, et al., Electroosmotic decontamination of concrete, in: United States. P. Medium vol. 73, Size, 1993.
[15] K.I. Popov, et al., Removal of cesium from the porous surface via the electrokinetic method in the presence of a chelating agent, Colloid J. 68 (6) (2006) 743–748.
[16] K. Popov, et al., Electrokinetic remediation of concrete: effect of chelating agents, Environ. Pollut. 153 (1) (2008) 22–28.
[17] M. Castellote, C. Andrade, C. Alonso, Nondestructive decontamination of mortar and concrete by electro-kinetic methods: application to the extraction of radioactive heavy metals, Environ. Sci. Technol. 36 (10) (2002) 2256–2261.
[18] D.W. DePaoli, M.T. Harris, M.R. Ally, Testing and evaluation of electrokinetic decontamination of concrete, in: United States. P. Medium, Size, 1996, p. 133.
[19] F. Frizon, S. Lorente, C. Auzuech, Nuclear decontamination of cementitious materials by electrokinetics: an experimental study, Cement Concr. Res. 35 (10) (2005) 2018–2025.
[20] G.N. Kim, W.K. Choi, K.W. Lee, Decontamination of radioactive concrete using electrokinetic technology, J. Appl. Electrochem. 40 (6) (2010) 1209–1216.
[21] G.N. Kim, et al., Washing-electrokinetic decontamination for concrete contaminated with cobalt and cesium, Nucl. Eng. Technol. 41 (8) (2009) 1079–1086.
[22] H. Lomasney, Electrokinetic Decontamination of Concrete, 1995. United States. p. 6.
[23] A. Anthofer, W. Lippmann, A. Hurtado, Laser decontamination of epoxy painted concrete surfaces in nuclear plants, Opt Laser. Technol. 57 (2014) 119–128.
[24] E. Arifi, et al., Reduction of contaminated concrete waste by recycling aggregate with the aid of pulsed power discharge, Construct. Build. Mater. 67 (2014) 192–196.
[25] Z. Bazant, G. Zi, Decontamination of radionuclides from concrete by microwave heating I: theory, J. Eng. Mech-asce - J ENG MECH-ASCE 129 (2003).
[26] A. Akbar Nezhad, K. Ong, Microwave decontamination of concrete, Mag. Concr. Res. 62 (2010) 879–885.
[27] T.L. White, et al., Removal of contaminated concrete surfaces by microwave heating: phase 1 results, in: Conference: Waste Management '92, Tucson, AZ, United States), 1992, 1-5 Mar 1992, United States. p. Medium: X; Size: Pages: (10 pp.).
[28] White, T.L., et al., Phase 2 microwave concrete decontamination results, in Conference: Waste Management '95, Tucson, AZ (United States), 26 Feb - 2 Mar 1995; Other Information: PBD: [1995]. 1995: United States. p. Medium: ED; Size: 11 p.
[29] M. Laraia, Nuclear Decommissioning: Planning, Execution and International Experience, Elsevier Science, 2012.
[30] D.C. Echert, M. Hashish, M.H. Marvin, Abrasive-waterjet Cutting of Thick Concrete and Waterjet Cleaning for Nuclear Facility Decommissioning and Decontamination, 1987, pp. VI80–VI94. United States.
[31] F. Moggia, et al., Nitrojet ® : a versatile tool for decontamination, Cut. Con. Scabbling. 11225 (2011).
[32] T. System, Concrete decontamination by electro-hydraulic scabbling (EHS). Final report, United States. p. Medium (1997). Size: 174.
[33] T.W. Lynch, Diamond Blade Grinding as a Means for Removing Surface Contamination from Concrete, United States, 1980, pp. 55–61.
[34] P. O'Sullivan, J.G. Nokhamzon, E. Cantrel, Decontamination and dismantling of radioactive concrete structures, NEA News 28 (2) (2010) 27–29.
[35] B.L. Woods, R.F. GoZsett, APPLICATION OF DIAMOND TOOLS WHEN DECONTAMINATING CONCRETE, 1980.
[36] K. Tatenuma, et al., Newly developed decontamination technology based on gaseous reactions converting to carbonyl and fluoric compounds, Nucl. Technol. 124 (2) (1998) 147–164.
[37] Y.S. Kim, S.H. Jeon, C.H. Jung, Fluorination reaction of uranium dioxide in CF4/O2/N2 r.f. plasma, Ann. Nucl. Energy 30 (11) (2003) 1199–1209.
[38] Y.-s. Kim, et al., Uranium dioxide reaction in CF4/O2 RF plasma, J. Nucl. Mater. 270 (1) (1999) 253–258.
[39] J.C. Martz, et al., Demonstration of plutonium etching in a CF4O2 RF glow discharge, J. Nucl. Mater. 182 (1991) 277–280.
[40] J.M. Veilleux, et al., Etching of UO2 in NF3 RF plasma glow discharge, J. Nucl. Mater. 277 (2) (2000) 315–324.
[41] H.F. Windarto, et al., Removal of oxide film prepared under BWR condition by using atmospheric CF4/O2 plasma decontamination process, J. Nucl. Sci. Technol. 37 (10) (2000) 913–918.
[42] X. Yang, , M.M., S.E. Babayan, G.R. Nowling, R.F. Hicks, Etching of uranium oxide with a non-thermal, atmospheric pressure plasma, J. Nucl. Mater. 324 (2004) 134–139.
[43] K. Fujiwara, et al., A new method for decontamination of radioactive waste using low-pressure arc discharge, Corrosion Sci. 48 (6) (2006) 1544–1559.
[44] Y.-H. Kim, et al., Decontamination of radioactive metal surface by atmospheric pressure ejected plasma source, Surf. Coating. Technol. 171 (2002) 317–320.
[45] Y.-s. Kim, Y.-d. Seo, M. Koo, Decontamination of metal surface by reactive cold plasma: removal of cobalt, J. Nucl. Sci. Technol. 41 (11) (2004) 1100–1105.
[46] S.H. Jeon, Y.s. Kim, A study on plasma etching reaction of cobalt for metallic surface decontamination, J. Korean Radioact. Waste Soc. 6 (1) (2008) 17–23.
[47] S.H. Jeon, Y.S. Kim, C.H. Jung, Cold plasma processing and plasma chemistry of metallic cobalt surface, Plasma Chem. Plasma Process. 28 (5) (2008) 617.
[48] J. Lee, K. Kim, Y.-S. Kim, A study on the NF3 plasma etching reaction with cobalt oxide grown on Inconel base metal surface, Plasma Chem. Plasma Process. 39 (4) (2019) 1145–1159.
[49] M. Achternbosch, et al., Heavy Metals in Cement and Concrete Resulting from the Co-incineration of Wastes in Cement Kilns with Regard to the Legitimacy of Waste Utilisation, 2003.
[50] D. Nicholls, 41 - cobalt, in: D. Nicholls (Ed.), The Chemistry of Iron, Cobalt and Nickel, Pergamon, 1973, pp. 1053–1107.
[51] T. Noguchi, Resource Recycling in Concrete: Present and Future, Stock Management for Sustainable Urban Regeneration, 2009, pp. 255–274.
[52] K.J. Clay, et al., Characterization of a-C:H:N deposition from CH4/N2 rf plasmas using optical emission spectroscopy, J. Appl. Phys. 79 (9) (1996) 7227–7233.
[53] N. Krstulović, et al., Optical emission spectroscopy characterization of oxygen plasma during treatment of a PET foil, J. Phys. Appl. Phys. 39 (17) (2006), 3799.
[54] R. Bogdanowicz, Investigation of H2:CH4 plasma composition by means of spatially resolved optical spectroscopy, Acta Phys. Pol., A 114 (6 A) (2008) A33–A38.
[55] N. Krstulović, et al., An optical-emission-spectroscopy characterization of oxygen plasma during the oxidation of aluminium foils, Materiali in Tehnologije 43 (5) (2009) 245–249.
[56] N.N. Greenwood, A. Earnshaw, Chemistry of the Elements, Elsevier Science, 2012.
[57] X. Niu, et al., NF3 decomposition over some metal oxides in the absence of water, J. Nat. Gas Chem. 19 (5) (2010) 463–467.
[58] R.D. Scheele, et al., Thermal NF3 fluorination/oxidation of cobalt, yttrium, zirconium, and selected lanthanide oxides, J. Fluor. Chem. 146 (2013) 86–97.
[59] J.F. Moulder, J. Chastain, Handbook of X-Ray Photoelectron Spectroscopy: A Reference Book of Standard Spectra for Identification and Interpretation of XPS Data, Physical Electronics Division, Perkin-Elmer Corporation, 1992.
[60] A.V. Naumkin, et al., NIST X-Ray Photoelectron Spectroscopy Database, 2012.
[61] W. Li, et al., Decomposition of CoF3 during battery electrode processing, J. Fluor. Chem. 205 (2018) 43–48.
[62] T.C. C, W. H.D, *Tungsten Etching in $CF_4$ and $SF_6$ discharges*, J. Electrochem. Soc. 131 (1) (1984) 115–120.
[63] S. El-Genk Mohamed, H. Saber Hamed, J. Veilleux, Analysis and modeling of decontamination experiments of depleted uranium dioxide in RF plasma, Ann. N. Y. Acad. Sci. 891 (1) (2006) 207–215.
[64] G.S. Oehrlein, Y. Kurogi, Sidewall surface chemistry in directional etching processes, Mater. Sci. Eng. R Rep. 24 (4) (1998) 153–183.
[65] A. Eksaeva, et al., Surface roughness effect on Mo physical sputtering and redeposition in the linear plasma device PSI-2 predicted by ERO2.0, Nuclear Mater. Energy. 19 (2019) 13–18.
[66] K.R. Williams, K. Gupta, M. Wasilik, Etch rates for micromachining processing-Part II, J. Microelectromech. Syst. 12 (6) (2003) 761–778.
[67] D. Flamm, C. Mogab, E. Sklaver, Reaction of fluorine atoms with SiO2, J. Appl. Phys. 50 (10) (1979) 6211–6213.
[68] X. Li, et al., Surface chemical changes of aluminum during NF 3-based plasma processing used for in situ chamber cleaning, J. Vac. Sci. Technol.: Vacuum Surf. Film. 22 (1) (2004) 158–164.